

## Simulation of the interannual variations of tropospheric ozone over China: Roles of variations in meteorological parameters and anthropogenic emissions

Sijia Lou, Hong Liao\*, Yang Yang, Qing Mu

State Key Laboratory of Atmospheric Boundary Layer Physics and Atmospheric Chemistry (LAPC), Institute of Atmospheric Physics, Chinese Academy of Sciences, Beijing 100029, China



### HIGHLIGHTS

- We quantify the interannual variations (IAVs) of tropospheric O<sub>3</sub> concentrations in China.
- The roles of variations in meteorological parameters and anthropogenic emissions are examined.
- Surface-layer O<sub>3</sub> concentrations over NC, SC, and SCB have IAVs of 0.7–3.9%, 1.4–3.7%, and 2.7–3.8%, respectively.
- Variations in winds are found to have the largest impact on the IAVs of O<sub>3</sub> over NC, SC, and SCB.

### ARTICLE INFO

#### Article history:

Received 10 March 2015

Received in revised form

24 August 2015

Accepted 26 August 2015

Available online 29 August 2015

#### Keywords:

Tropospheric ozone

Interannual variation

Process analysis

China

### ABSTRACT

We quantify the interannual variations (IAVs) of tropospheric O<sub>3</sub> over China for the years 2004–2012 by using the one-way nested-grid version of the global three-dimensional Goddard Earth Observing System chemical transport model (GEOS-Chem). The roles of variations in meteorological fields and anthropogenic emissions of O<sub>3</sub> precursors are examined separately and together through sensitivity simulations. With variations in both meteorological parameters and emissions, simulated seasonal mean surface-layer O<sub>3</sub> concentrations over North China (NC, 110–120°E, 32–42°N) exhibit the largest IAVs in June–July–August (JJA). The regionally averaged absolute percent departure from the mean (APDM) values over NC are 0.7%, 3.2%, 3.9%, and 2.1% in December–January–February (DJF), March–April–May (MAM), and September–October–November (SON), respectively. Over South China (SC, 110–120°E, 22–32°N), the IAVs of O<sub>3</sub> are found maximum in MAM, and minimum in JJA; the APDM values are 2.7%, 3.7%, 1.4%, and 2.6% in DJF, MAM, JJA, and SON, respectively. With respect to the IAVs of O<sub>3</sub> over the Sichuan Basin (SCB, 102–110°E, 27–33°N), the APDM values are simulated to be 2.7–3.8% throughout the year. The IAVs in surface-layer O<sub>3</sub> by variations in meteorological fields are simulated to be larger than those by variations in anthropogenic emissions throughout the year in NC and SC except for JJA in SC. The relatively more important role of variations in anthropogenic emissions is simulated in SCB in all seasons. Process analyses are performed to identify key meteorological parameters that influence the IAVs of O<sub>3</sub> over NC, SC, and SCB. Over all of these regions, variations in winds are found to have the largest impact on the IAVs of O<sub>3</sub>, followed by those in temperature and specific humidity. Considering that the APDM values represent the IAVs averaged over 2004–2012, the magnitudes of IAVs of O<sub>3</sub> for specific years can be more significant than the numbers reported here. Our results have important implications for the effectiveness of short-term air quality control strategies in China.

© 2015 The Authors. Published by Elsevier Ltd. This is an open access article under the CC BY-NC-ND license (<http://creativecommons.org/licenses/by-nc-nd/4.0/>).

### 1. Introduction

Tropospheric O<sub>3</sub> is a major air pollutant in the atmosphere that has adverse effects on human health and ecosystem productivity (UNEP, 2006; Shindell et al., 2012). It is also an important greenhouse gas with a global mean radiative forcing of 0.4 (0.2–0.6) W

\* Corresponding author.

E-mail address: [hongliao@mail.iap.ac.cn](mailto:hongliao@mail.iap.ac.cn) (H. Liao).

$\text{m}^{-2}$  (Intergovernmental Panel on Climate Change (IPCC, 2013)). High  $\text{O}_3$  concentrations have been observed in China, with seasonal mean concentrations of 20–60 ppbv (parts per billion by volume; Xu et al., 2008; Yang et al., 2008; Zhang et al., 2008; Wang et al., 2011)) and episodic  $\text{O}_3$  concentrations of exceeding 100 ppbv (Wang et al., 2006; Duan et al., 2008; Ge et al., 2012). Ozone concentrations exhibit variations on different time scales, from days to decades (Pozzoli et al., 2011; Fu et al., 2012; Yang et al., 2014). In this work we aim to quantify the interannual variations (IAVs) of tropospheric  $\text{O}_3$  and examine the drivers (either variations in meteorological parameters or in emissions) of the IAVs. Such studies can help with interpretation of year-by-year variations in  $\text{O}_3$  measurements and understanding of the effectiveness of short-term air quality control strategies. For example, if the IAVs of  $\text{O}_3$  driven by variations in meteorological parameters are larger than those caused by variations in emissions, the short-term air quality control may need extra efforts to reduce emissions if the meteorological parameters are not favorable for  $\text{O}_3$  air quality.

The absolute IAVs of  $\text{O}_3$  can be quantified by standard deviation (SD) and mean absolute deviation (MAD), defined as

$$\text{SD} = \sqrt{\frac{1}{n} \sum_{i=1}^n \left( C_i - \frac{1}{n} \sum_{i=1}^n C_i \right)^2} \quad \text{and} \quad \text{MAD} = \frac{1}{n} \sum_{i=1}^n \left| C_i - \frac{1}{n} \sum_{i=1}^n C_i \right|,$$

respectively, while the IAVs relative to the multi-year average of concentrations can be quantified by relative standard deviation (RSD) and absolute percent departure from the mean (APDM), defined as  $\text{RSD} = 100\% \times \text{SD} / \left( \frac{1}{n} \sum_{i=1}^n C_i \right)$  and  $\text{APDM} =$

$100\% \times \text{MAD} / \left( \frac{1}{n} \sum_{i=1}^n C_i \right)$ , where  $C_i$  is the observed or simulated  $\text{O}_3$  concentration in year  $i$ , and  $n$  represents the number of years examined.

Previous studies have reported the IAVs of tropospheric  $\text{O}_3$  for different regions. Liu et al. (2011) found that simulated July  $\text{O}_3$  concentrations at 400 hPa over the Middle East over 1987–2006 had SD and RSD values of 6 ppbv and 7%, respectively, by using the GEOS-Chem model with a horizontal resolution of  $4^\circ$  latitude by  $5^\circ$  longitude. Pozzoli et al. (2011) examined the global mean concentrations of pollutants simulated for years of 1980–2005 from the coupled aerosol-chemistry-climate model ECHAM5-HAMMOZ with a horizontal resolution of  $2.8^\circ \times 2.8^\circ$ . They found that the global mean surface-layer  $\text{O}_3$  exhibited SD and RSD values of 0.83 ppbv and 2.3% with changes in anthropogenic emissions and of 0.63 ppbv and 1.7% with fixed anthropogenic emissions. Kumar et al. (2013) compared  $\text{O}_3$  concentrations observed at the Pico Mountain Observatory (PMO) (at an altitude of 2225 m) with those simulated from the GEOS-Chem model for years of 2004–2010, and found that the averaged  $\text{O}_3$  concentrations over May–August from observations and simulations exhibited MAD (APDM) values of 1.1 ppbv (2.7%) and 1.1 ppbv (2.4%), respectively. Sahu et al. (2014), by analyzing Measurement of Ozone and Water Vapor by Airbus In-Service Aircraft (MOZAIC) datasets during 2006–2008 over Hyderabad and India, reported that  $\text{O}_3$  concentrations averaged over the premonsoon season (March–May) had large IAVs, with values of 58 ppbv in 2006 and 44 ppbv in 2008 in the lower troposphere (2–4 km) depending on the transport of marine and continental air and values of 72 ppbv in 2006 and 50 ppbv in 2008 in the upper troposphere (8–11 km) depending on deep convections.

Observational and modeling studies have also illustrated that surface-layer  $\text{O}_3$  have large IAVs over China. Tang et al. (2009) showed that, on the basis of measurements at 6 sites in downtown Beijing for years of 2001–2006, the average  $\text{O}_3$  concentrations over July–September in Beijing exhibited APDM value of 3.6%.

Zhang et al. (2013) analyzed  $\text{O}_3$  measurements in Hong Kong over the period of 1999–2011, and reported that the seasonal mean  $\text{O}_3$  concentrations had MAD and APDM values of 3–6 ppbv and 9–18%, respectively. They also reconstructed the time series of  $\text{O}_3$  by taking into account the IAVs in frequency and intensity of circulation patterns. Such reconstruction captured up to 50% of the observed IAV of  $\text{O}_3$ , suggesting that the changes in meteorological parameters have large impacts on the IAVs of surface  $\text{O}_3$  levels in Hong Kong.

The concentrations of  $\text{O}_3$  are dependent on both precursor emissions and meteorological conditions. Meteorological parameters influence  $\text{O}_3$  concentrations by altering cross stratosphere–troposphere flux of  $\text{O}_3$  (Voulgarakis et al., 2011; Hess and Zbinden, 2013), biogenic emission of volatile organic compounds (Fu and Liao, 2012), and the chemical production and loss, transport, and deposition of  $\text{O}_3$  (Lin et al., 2001; Camalier et al., 2007; Ramsey et al., 2014). Olsen et al. (2013) estimated the extratropical stratosphere–troposphere exchange of  $\text{O}_3$  from 2005 to 2010 by combining Microwave Limb Sounder (MLS) ozone observations with Modern Era Retrospective-Analyses for Research and Applications (MERRA) of meteorological fields, and found that the difference between the highest annual flux in 2006 and the lowest annual flux in 2008 was about 15% of the multiyear mean STE (Strat-Trop exchange) in the Northern Hemisphere. Neu et al. (2014) used Aura satellite measurements (from Tropospheric Emission Spectrometer (TES) and MLS instruments) of stratospheric water and tropospheric  $\text{O}_3$  levels for years of 2005–2010 to quantify the impact of changes in the stratospheric circulation on tropospheric  $\text{O}_3$ . They reported that a 25% increase in stratospheric  $\text{O}_3$  results in a 2% increase in 500 hPa  $\text{O}_3$  in the northern mid-latitudes, approximately half of the interannual tropospheric  $\text{O}_3$  variability, based on CAM-Chem simulation. Variations in temperature and water vapor in the atmosphere also influence production and loss of  $\text{O}_3$ . Dawson et al. (2007) found that the daily maximum 8-h  $\text{O}_3$  concentrations increase with temperature by about 0.34 ppbv  $K^{-1}$  and decrease by 0.025 ppbv for each percent increase in absolute humidity over eastern United States during July 12–21, 2001, by using the PMCAMx model with perturbations of individual meteorological parameters. Furthermore, climate patterns, such as monsoon and El Nino, play important roles in the IAVs of  $\text{O}_3$  concentrations (Neu et al., 2014; Sahu et al., 2014; Sekiya and Sudo, 2014; Yang et al., 2014).

The major processes that influence the concentrations of  $\text{O}_3$  include horizontal and vertical transport, chemical production and loss, dry and wet deposition. The role of each physical or chemical process can be quantified by the Integrated Process Rate (IPR) analysis. Such approach has been applied to episodic events (Jose et al., 2002; Goncalves et al., 2009; Im et al., 2011), and yearly to decadal simulations (Zhang et al., 2009b; Civerolo et al., 2010). For example, Goncalves et al. (2009) found that the formation of surface  $\text{O}_3$  was dominated by the horizontally advected flows and gas-phase chemical reactions occurring aloft in the morning, and by vertical advective flows in the afternoon and dusk, during a photochemical pollution episode over southern Mediterranean region in summer. Similar process analyses were also implemented in other models, such as the Weather Research and Forecasting model coupled with Chemistry (WRF-Chem, Jiang et al., 2012; Jiang et al., 2013) and the GEOS-Chem model (Mu and Liao, 2014), to understand the key processes that influence the concentrations or variations of  $\text{O}_3$  and aerosols.

This work aims to (1) quantify the IAVs of tropospheric  $\text{O}_3$  concentrations in China due to the variations in meteorological fields and/or anthropogenic emissions during 2004–2012 using the GEOS-Chem model driven by the assimilated meteorological fields, and (2) identify the dominant meteorological parameters that

influence the IAVs of O<sub>3</sub> in different polluted regions in China, by an application of IPR analysis. We are focused especially on the IAVs of O<sub>3</sub> over the three polluted regions, including North China (NC, 110–120°E, 32–42°N), South China (SC, 110–120°E, 22–32°N), and the Sichuan Basin (SCB, 102–110°E, 27–33°N). This study is a companion study to the work of Mu and Liao (2014), which investigated the interannual variations of aerosols in China.

The description of model and numerical experiments is presented in Section 2. Simulated IAVs in seasonal mean O<sub>3</sub> concentrations are presented and evaluated in Section 3, with the roles of variations in meteorological fields and emissions examined. The key meteorological parameters that drive the IAVs of O<sub>3</sub> are identified by process analyses in Section 4. The impacts of O<sub>3</sub> flux from STE on the IAVs of O<sub>3</sub> in China are discussed in Section 5.

## 2. Model description and numerical experiments

### 2.1. GEOS-Chem model

We simulate tropospheric O<sub>3</sub> concentrations in China using the one-way nested-grid version of the global chemical transport model GEOS-Chem (version 9-01-02, <http://acmg.seas.harvard.edu/geos/>) driven by the GEOS-5 assimilated meteorological fields from the Goddard Earth Observing System of the NASA Global Modeling and Assimilation Office (GMAO). The version of the model used here has a nested horizontal resolution of 0.5° latitude by 0.667° longitude over East Asia (70°–150°E, 11°S–55°N) and 47 vertical layers up to 0.01 hPa. Tracer concentrations at the lateral boundaries are obtained from the global GEOS-Chem simulations performed at 4° latitude by 5° longitude horizontal resolution and updated in the nested-grid simulations every 3 h (Chen et al., 2009).

The GEOS-Chem model includes a fully coupled simulation of O<sub>3</sub>-NO<sub>x</sub>-VOC chemistry (Bey et al., 2001) and aerosols including SO<sub>4</sub><sup>2-</sup>/NO<sub>3</sub><sup>-</sup>/NH<sub>4</sub><sup>+</sup> (Park et al., 2004; Pye et al., 2009), BC and OC (Park et al., 2003), mineral dust (Fairlie et al., 2007) and sea salt (Alexander et al., 2005). Tropospheric O<sub>3</sub> is simulated with about 80 species and over 300 chemical reactions (Bey et al., 2001). The cross-tropopause O<sub>3</sub> flux in the GEOS-Chem model is specified with the linearized ozone (Linoz) or synthetic ozone (Synoz) method (McLinden et al., 2000). Linoz is a first-order Taylor expansion of stratospheric chemical rates in which the O<sub>3</sub> tendency has been linearized about the local O<sub>3</sub> mixing ratio, temperature, and the overhead column O<sub>3</sub> density. Synoz is a passive, ozone-like tracer released into the stratosphere at a rate equivalent to that of the cross-tropopause O<sub>3</sub> flux of 499 Tg yr<sup>-1</sup>. The GEOS-Chem model accounts for the impacts of aerosols on distributions and concentrations of O<sub>3</sub> through heterogeneous reactions and changes in photolysis rates (Lou et al., 2014).

### 2.2. Emissions

Global emissions of O<sub>3</sub> precursors, aerosol precursors and aerosols in the GEOS-Chem model generally follow Park et al. (2003, 2004). Anthropogenic emissions of CO, NO<sub>x</sub>, SO<sub>2</sub>, NH<sub>3</sub>, and non-methane volatile organic compounds (NMVOCs), including emissions from power, industry, residential biofuel/fossil fuel/non-combustion, and transportation) over East Asia are overwritten by the David Streets' 2006 emission inventory (Zhang et al., 2009a) in this work. The IAVs in anthropogenic emissions are represented by annual scaling factors. The global annual scaling factors are obtained following the approach described by Van Donkelaar et al. (2008), according to numerous sources and directly use government statistics where available. For IAVs in anthropogenic emissions over 2004–2012 in China, the annual scaling factors for

aerosol precursors (NO<sub>x</sub>, SO<sub>2</sub>, OC, and BC) follow Mu and Liao (2014), for CO are taken from Yumimoto et al. (2014), and for NMVOCs are taken from Wei et al. (2014). Biomass burning emissions with interannual variations are taken from the monthly Global Fire Emissions Database-v3 (GFED3) inventory (van der Werf et al., 2010). The scaling factors for IAVs in anthropogenic emissions are spatially heterogeneous outside China. Within China, the scaling factors for a chemical species are the same at all the grid cells.

The biogenic emissions in the GEOS-Chem model are simulated using the Model of Emissions of Gases and Aerosols from Nature version 2.1 (MEGAN2.1) module (Guenther et al., 2012). Natural NO<sub>x</sub> emissions from soil are computed using a modified version of the algorithm proposed by Yienger and Levy (1995), and those from lightning follow the scheme described by Sauvage et al. (2007) and Murray et al. (2012). Table 1 summarizes the interannual variations of annual emissions of NO<sub>x</sub>, CO, and NMVOCs in eastern China (100–126°E, 20–50°N) for years of 2004–2012, including emissions from both anthropogenic and natural sources.

### 2.3. Numerical experiments

The concentrations of O<sub>3</sub> in China for years 2004–2012 are simulated using the GEOS-Chem model driven by the GEOS-5 meteorological fields. To identify the relative importance of parameters or processes that influence the IAVs of O<sub>3</sub>, we perform the following simulations:

- (1) CTRL: The standard simulation of O<sub>3</sub> concentrations over 2004–2012 with IAVs in both meteorological fields and emissions (including anthropogenic, natural, and biomass emissions). LINOZ method is used to calculate the cross-tropopause O<sub>3</sub> flux, which can account for the IAVs of STE of O<sub>3</sub>.
- (2) MET: The sensitivity simulation of O<sub>3</sub> concentrations over 2004–2012 to quantify the impacts of variations in meteorological parameters on the IAV of O<sub>3</sub>. Anthropogenic emissions and biomass emissions are fixed at year 2006 levels. Meteorological fields and natural emissions are allowed to vary over 2004–2012. LINOZ method is used to calculate the cross-tropopause O<sub>3</sub> flux.
- (3) AEMIS: The sensitivity simulation of O<sub>3</sub> concentrations over 2004–2012 to quantify the impacts of variations in anthropogenic emissions on the IAV of O<sub>3</sub>. Year 2006 meteorological fields are used to drive the simulation (natural emissions are therefore fixed at the year 2006 levels). Anthropogenic emissions are allowed to vary over 2004–2012. Biomass burning emissions are fixed at the year 2006 levels and LINOZ method is used to calculate the cross-tropopause O<sub>3</sub> flux.

**Table 1**

Annual emissions O<sub>3</sub> precursors in eastern China (100–126°E, 20–50°N) for years of 2004–2012.

Year	NO <sub>x</sub> (Tg N yr <sup>-1</sup> )	CO (Tg CO yr <sup>-1</sup> )	NMVOCs (Tg C yr <sup>-1</sup> )
2004	5.3	130.7	24.5
2005	6.1	131.7	25.2
2006	6.6	171.7	26.7
2007	6.9	168.7	27.9
2008	6.8	169.9	27.0
2009	7.2	166.9	27.3
2010	7.6	166.6	27.3
2011	7.9	164.7	26.9
2012	8.3	162.9	26.5

- (4) AEMISB: The sensitivity simulation of O<sub>3</sub> concentrations over 2004–2012 to quantify the impacts of variations in biomass burning emissions on the IAV of O<sub>3</sub>. This simulation is the same as AEMIS except that biomass burning emissions are allowed to vary over 2004–2012. LINOZ method is used to calculate the cross-tropopause O<sub>3</sub> flux.
- (5) TROP: The sensitivity simulation of O<sub>3</sub> concentrations over 2004–2012 to quantify the impacts of STE on the IAVs of O<sub>3</sub>. This simulation is the same as MET except that SYNOZ is used to calculate the cross-tropopause O<sub>3</sub> flux. Therefore STE of O<sub>3</sub> is fixed at 499 Tg yr<sup>-1</sup> during the integration over 2004–2012.

Comparison of the IAVs of O<sub>3</sub> in MET with those in AEMIS identifies the relative importance of variations in meteorological conditions and anthropogenic precursor emissions in the IAVs of tropospheric O<sub>3</sub>. The differences between AEMISB and AEMIS show the impact of variations in biomass burning emissions on the IAVs of O<sub>3</sub>, and the differences between MET and TROP represent the IAV of O<sub>3</sub> caused by STE.

### 3. Simulated IAVs of O<sub>3</sub> in China

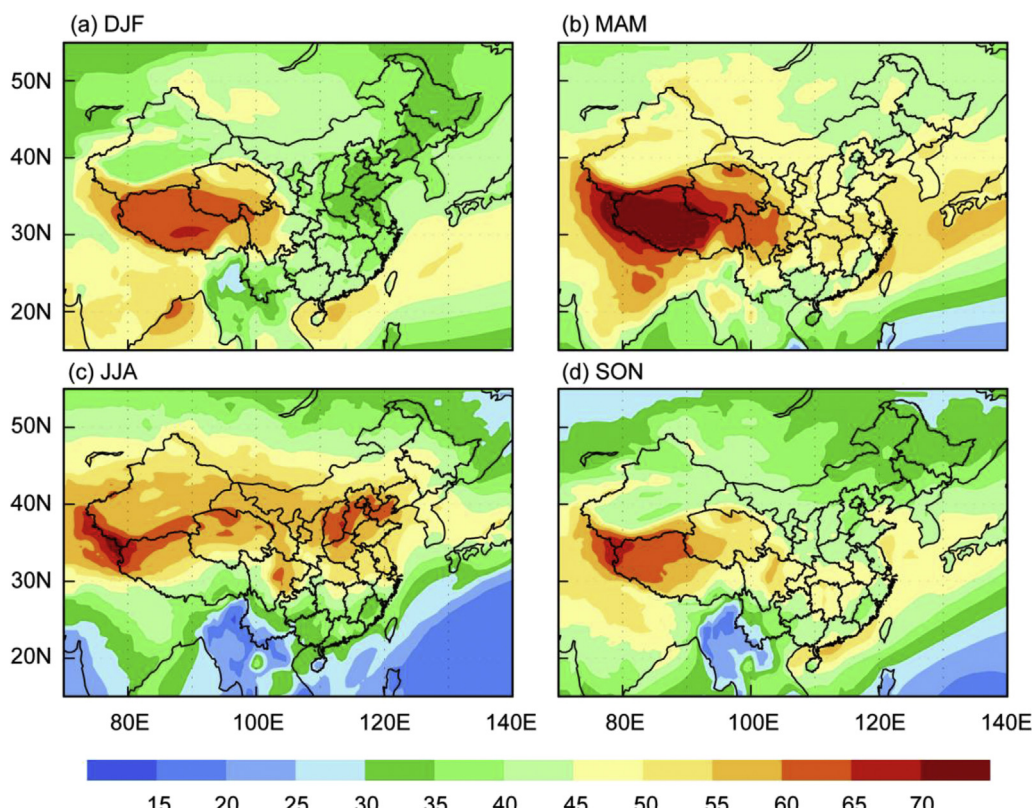
#### 3.1. Simulated O<sub>3</sub> concentrations in China

Figure 1 shows the simulated seasonal mean surface-layer concentrations of O<sub>3</sub> averaged over the period 2004–2012 from the CTRL simulation with variations in both meteorology and emissions. Over eastern China, seasonal mean O<sub>3</sub> concentrations are the lowest in December–January–February (DJF) with values of 25–45 ppbv due to the weak photochemistry. In March–April–May (MAM) and September–October–November (SON), O<sub>3</sub> concentrations in eastern China are simulated in the ranges of

40–55 and 35–50 ppbv, respectively. The maximum O<sub>3</sub> concentrations of 55–65 ppbv are simulated in JJA in the northern China. Over the Tibet Plateau, simulated O<sub>3</sub> exhibits maximum concentrations of exceeding 70 ppbv in MAM because of the transport of O<sub>3</sub> from the stratosphere to troposphere (Wild and Akimoto, 2001).

#### 3.2. Simulated IAVs of O<sub>3</sub>

Figures 2a and 3a show the MAD and APDM values of seasonal mean surface-layer O<sub>3</sub> concentrations from the CTRL simulation, respectively. The IAVs of O<sub>3</sub> are large throughout the year over the Tibet Plateau, especially in JJA when the MAD and APDM values exceed 3 ppbv and 8%, respectively. The large IAVs in JJA in the Tibet Plateau are associated with the IAVs of East Asian summer monsoon (Yang et al., 2014). Over eastern China, surface-layer O<sub>3</sub> showed APDM values of 1–6%. The seasonal mean O<sub>3</sub> concentrations show the largest IAVs of 2.3 ppbv (3.9%) in JJA in NC, 1.8 ppbv (3.7%) in MAM in SC, and 1.9 ppbv (3.8%) in JJA in SCB (Table 2). With respect to the IAVs of O<sub>3</sub> over SCB, the values are simulated in the range of 1.8–2.0 ppbv (3.7–3.8%) throughout the year, except for 1.2 ppbv (2.7%) in DJF. Considering that the APDM values represent the IAVs averaged over 2004–2012, the magnitudes of the IAVs of O<sub>3</sub> for specific years can be more significant. Figure 4 shows the deviation from the mean for seasonal mean O<sub>3</sub> concentrations obtained in the CTRL simulation for 2004–2012. The deviation from the mean is defined as  $DM_i = \left( C_i - \frac{1}{n} \sum_{i=1}^n C_i \right) / \frac{1}{n} \sum_{i=1}^n C_i$ , where  $C_i$  is the simulated O<sub>3</sub> in year  $i$ , and  $n$  is the number of years examined ( $n = 9$  for years 2004–2012). The deviations from the mean are in the range of −7.0% to +7.5%, −6.0 to +6.0%, and −9.6 to +7.0% over NC, SC, and SCB, respectively.



**Fig. 1.** Simulated seasonal-mean surface-layer concentrations (ppbv) of O<sub>3</sub> averaged over 2004–2012 of the CTRL simulation.

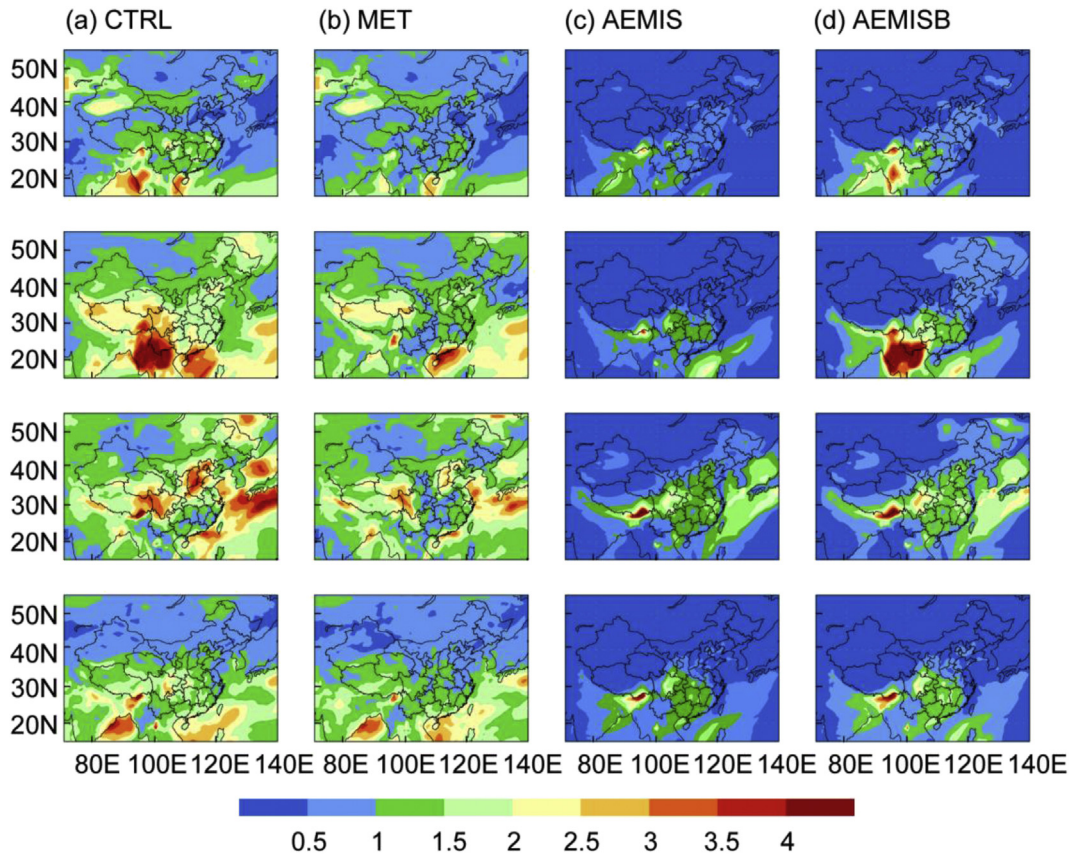


**Fig. 2.** Mean absolute deviation (MAD, ppbv) of surface-layer O<sub>3</sub> concentrations obtained from simulations of (a) CTRL, (b) MET, (c) AEMIS, and (d) AEMISB for years of 2014–2012.

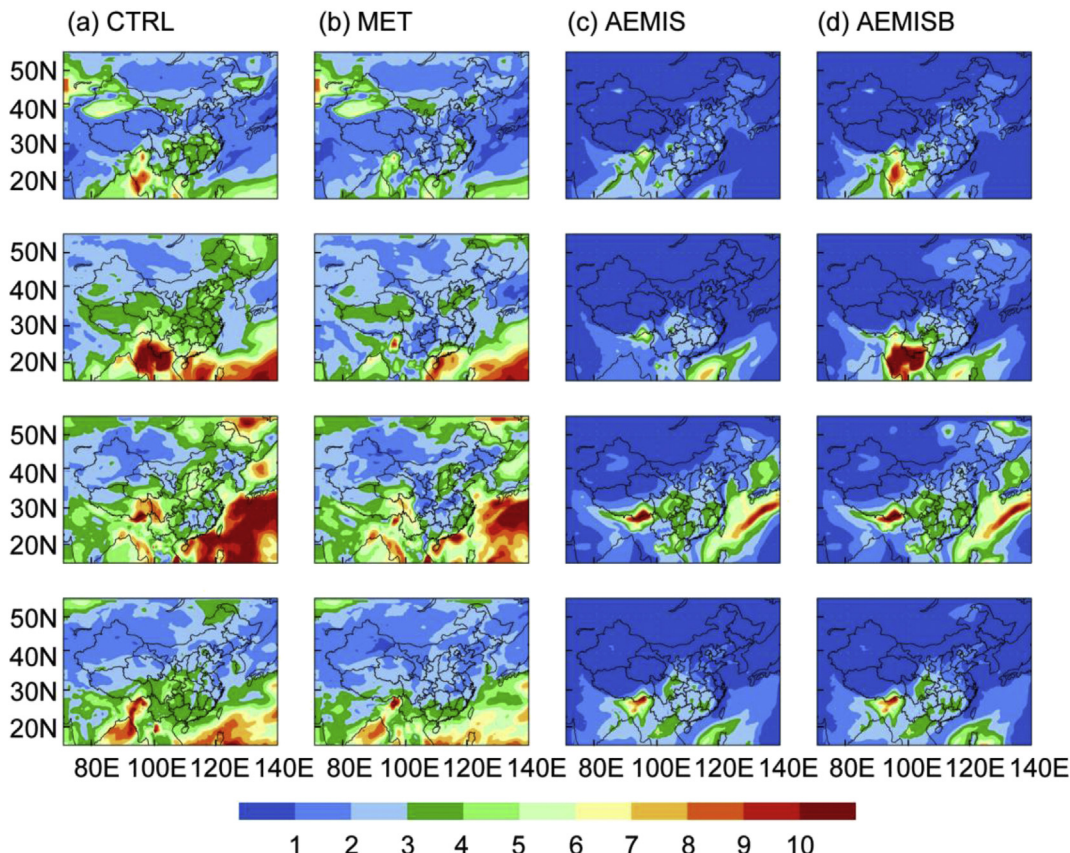


**Fig. 3.** Absolute percent departure from the mean (APDM, %) of surface-layer O<sub>3</sub> concentrations obtained from simulations of (a) CTRL, (b) MET, (c) AEMIS, and (d) AEMISB for years of 2004–2012.

**Table 2**

The MAD and APDM values of seasonal mean surface-layer O<sub>3</sub> concentrations averaged over the regions of NC, SC, and SCB. Results from the CTRL, MET, and AEMIS simulations are all shown for comparisons.

		NC			SC			SCB		
		CTRL	MET	AEMIS	CTRL	MET	AEMIS	CTRL	MET	AEMIS
MAD (ppbv)	DJF	0.2	0.4	0.4	1.1	0.9	0.4	1.2	0.7	0.8
	MAM	1.5	1.2	0.3	1.8	1.2	0.7	2.0	0.9	1.2
	JJA	2.3	1.4	1.0	0.6	0.8	1.0	1.9	0.9	1.8
	SON	0.9	0.7	0.4	1.2	1.1	0.9	1.8	0.8	1.4
APDM (%)	DJF	0.7%	1.2%	1.1%	2.7%	2.2%	0.9%	2.7%	1.5%	1.7%
	MAM	3.2%	2.6%	0.6%	3.7%	2.4%	1.4%	3.7%	1.6%	2.3%
	JJA	3.9%	2.4%	1.9%	1.4%	2.0%	2.4%	3.8%	1.8%	3.6%
	SON	2.1%	1.6%	0.9%	2.6%	2.5%	1.9%	3.8%	1.6%	2.8%

Our simulated IAVs of O<sub>3</sub> concentrations are close to the APDM values of 2–5% over eastern China simulated for JJA O<sub>3</sub> over years 1986–2006 (Yang et al., 2014), and the APDM value of 3.6% over

downtown Beijing on the basis of measurements of O<sub>3</sub> in July–September during 2001–2006 (Tang et al., 2009). These IAVs of O<sub>3</sub> are significant as compared to the changes in O<sub>3</sub> concentrations caused by decadal-scale climate change. For example, Jiang et al. (2008) showed that future climate change under the IPCC A1B scenario lead to increases in daily maximum 8-h O<sub>3</sub> concentrations in Houston by 2.6 ppbv over 2001–2051. The importance of the IAVs of O<sub>3</sub> can also be demonstrated when they are compared with the changes in O<sub>3</sub> concentrations simulated with reductions in emissions. The importance of the IAVs of O<sub>3</sub> can also be demonstrated when they are compared with the changes in O<sub>3</sub> concentrations simulated with reductions in emissions. While the deviation from the mean varies by about 15% from the year with the lowest O<sub>3</sub> concentration to that with the highest O<sub>3</sub> level (Fig. 4), 10–20% reduction in summer O<sub>3</sub> concentrations over eastern China requires 50% reductions in emissions of NO<sub>x</sub> or VOCs (anthropogenic plus biogenic VOCs) (Han et al., 2005).

### 3.3. Comparisons of simulated IAVs of O<sub>3</sub> with measurements

Simulated concentrations of O<sub>3</sub> in China using the one-way nested-grid capability of the GEOS-Chem have been evaluated in studies of Wang et al. (2011) and Lou et al. (2014). The model has been demonstrated to capture well the magnitude and seasonal variation of surface-layer and column burdens of O<sub>3</sub> in China (Wang et al., 2011), with an average bias of +9% at 14 sites (Lou et al., 2014). Since long-term O<sub>3</sub> observations are limited in China, we evaluate the IAVs in annual mean surface-layer O<sub>3</sub> concentrations simulated from the CTRL simulation at four sites (Fig. 5): Tap Mum (114.4°E, 22.5°N) in Hong Kong, Waliguan (100.9°E, 36.3°N) in China, Everest-Pyramid (86.8°E, 28.0°N) in Nepal, and Ryori (141.8°E, 39.0°N) in Japan. The measurements at Tap Mum are taken from Zhang et al. (2013), and those at the Waliguan, Everest-Pyramid, and Ryori sites are from the WMO (World Meteorological Organization) World Data Center for Greenhouse Gases (WDCGG, <http://ds.data.jma.go.jp/gmd/wdcgg/>). At Tap Mum, Everest-Pyramid, and Ryori sites, simulated O<sub>3</sub> concentrations are higher than the observations, which agree with previous modeling studies (Chatani and Sudo, 2011; Wang et al., 2011; Yang et al., 2014). The discrepancy at Ryori station is probably caused by the model's overestimation of O<sub>3</sub> in marine boundary layers in summer (Liu et al., 2006) and the model's inability to simulate cloud optical properties associated with the East Asian summer monsoon (Wang et al., 2008). The observed interannual peaks and troughs are captured fairly well by the model; the correlation coefficients between simulated and observed concentrations are +0.78, +0.52, and +0.47 at Tap Mum, Everest-Pyramid, and Ryori, respectively. At Waliguan, surface O<sub>3</sub> concentrations are influenced by both the transport from the stratosphere (Ding and Wang, 2006; Zheng et al., 2011) and anthropogenic emissions (Li et al., 2009). The

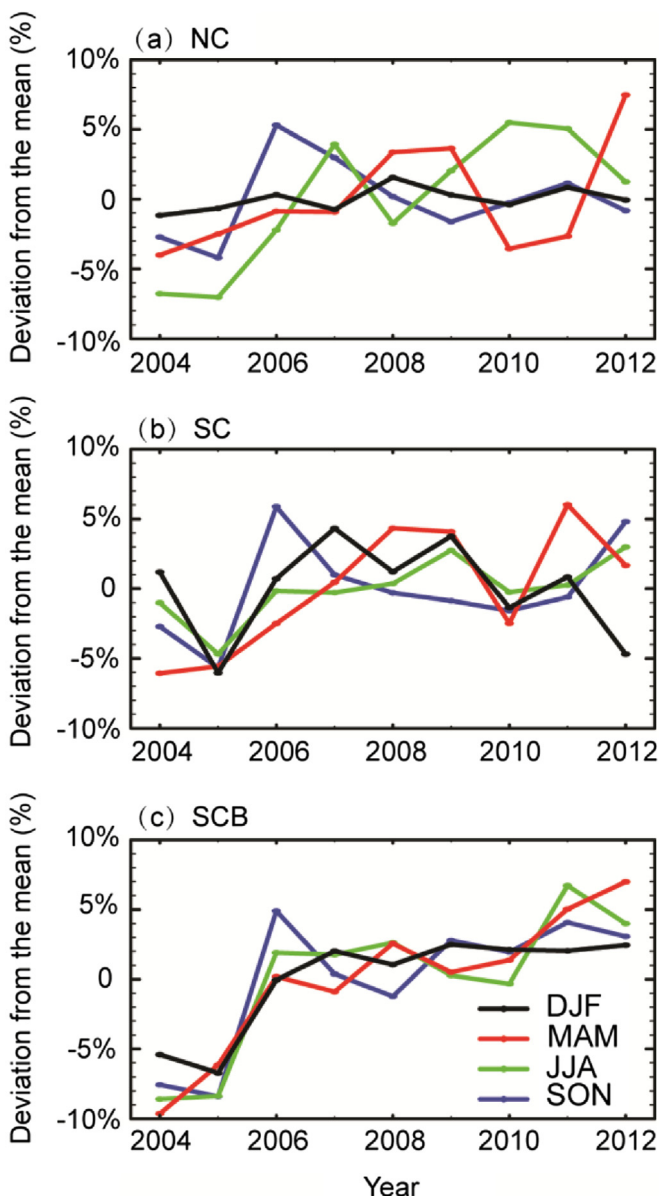


**Fig. 4.** Deviation from the mean for seasonal mean O<sub>3</sub> concentrations averaged over (a) NC, (b) SC, (c) SCB from the CTRL simulation.

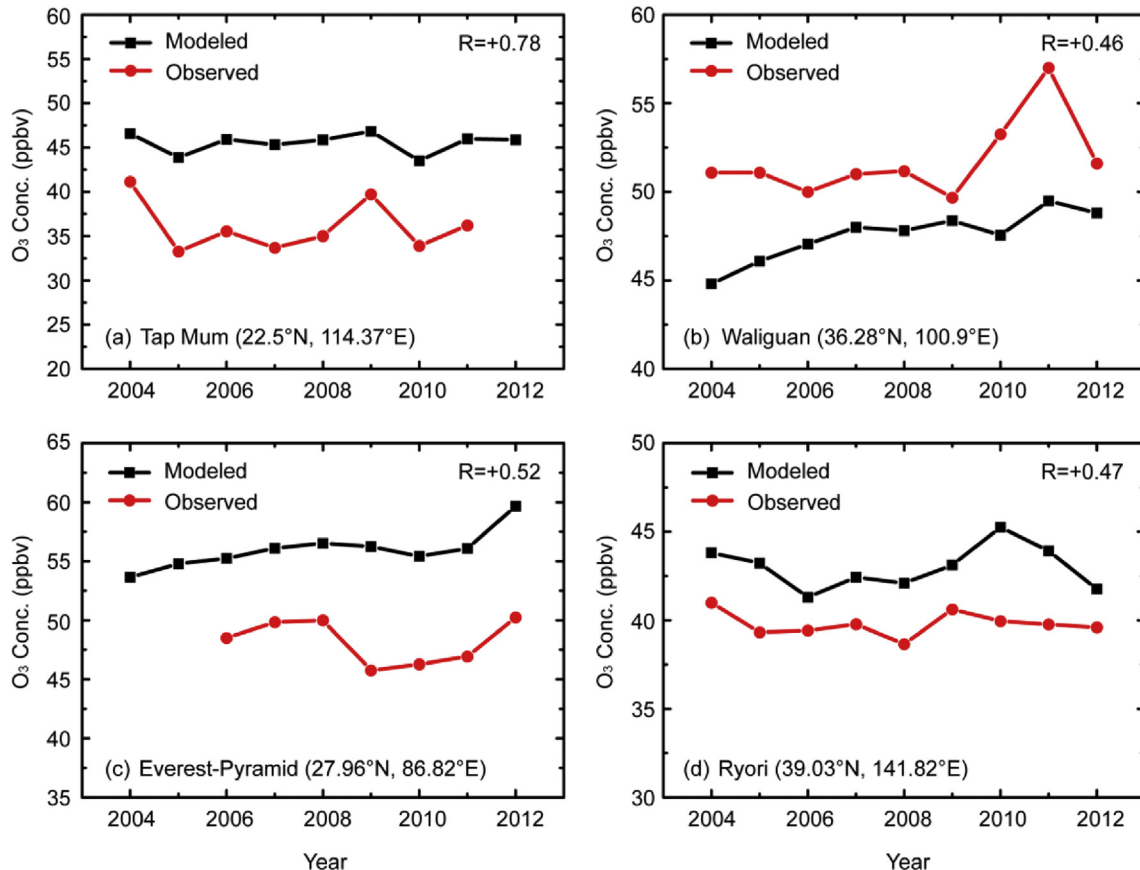


**Fig. 5.** Comparisons of observed and simulated annual mean surface-layer O<sub>3</sub> concentrations at (a) Tap Mum (114.37°E, 22.5°N) in Hong Kong, China, (b) Waliguan (100.9°E, 36.28°N) in western China, (c) Everest-Pyramid (86.82°E, 27.96°N) in Nepal, and (d) Ryori (141.82°E, 39.03°N) in Japan. Correlation coefficient (R) between simulated and observed concentrations is shown in each panel, which is calculated over the time period with observations available.

low biases in simulated annual mean O<sub>3</sub> concentration and the relatively low correlation coefficient of +0.46 at Waliguan may be influenced by the representation of these two processes in the model. The simulated annual APDM values at Tap Mum, Waliguan, Everest-Pyramid, and Ryori are 1.9%, 2.2%, 1.9%, and 2.3%, respectively, smaller than the observed IAVs of 4.5%, 2.5%, 3.8%, and 3.6% at these four sites, due to the model's underestimate of peak values and overestimate of low O<sub>3</sub> levels. Hogrefe et al. (2011) also found that the CMAQ/STATIC model underestimated high O<sub>3</sub> values and overestimated low observed values as the simulated O<sub>3</sub> concentrations were compared with observations over 1988–2005 from the US EPA Air Quality System.

#### 3.4. Impacts of changes in meteorological parameters or emissions on simulated IAVs of O<sub>3</sub>

The MAD and APDM values of seasonal mean surface-layer O<sub>3</sub> concentrations from simulations MET, AEMIS, and AEMISB are also shown in Figures 2 and 3, respectively. Averaged over NC, the variations in meteorological parameters alone (MET simulation) lead to the relatively large IAVs of O<sub>3</sub> in MAM and JJA with regional mean MAD (APDM) values of 1.2 ppbv (2.6%) and 1.4 ppbv (2.4%), respectively (Figs. 2b and 3b, Table 2). The variations in meteorological fields lead to larger IAVs of O<sub>3</sub> than those in anthropogenic emissions in NC in all seasons. Over SC, the variations in meteorological parameters lead to IAVs of O<sub>3</sub> of 2.2–2.5% in DJF, MAM, and SON, which are larger than the IAVs of 0.9–1.9% in these seasons owing to the variations in anthropogenic emissions. However,

the variations in anthropogenic emissions are more important in SC in JJA, with regional mean MAD (APDM) values of 1.0 ppbv (2.4%) in AEMIS simulation and of 0.8 ppbv (1.9%) in MET simulation. The relatively more important role of variations in anthropogenic emissions is also simulated in SCB; averaged over SCB, the variations in meteorological parameters lead to IAVs of O<sub>3</sub> of 1.5–1.8%, which are smaller than the IAVs of 1.7–3.6% in AEMIS simulation (Table 2). Over western China, the variations in meteorological parameters are simulated to be the dominant factor that led to IAVs of O<sub>3</sub> in all seasons because of the small anthropogenic emissions over there.

The impacts of variations in biomass burning emissions on the IAVs of O<sub>3</sub> can be identified by comparing results from simulations AEMISB and AEMIS. Large biomass burning events often occur in Southeast Asia during springtime because of the agriculture cleanup activities (Newell et al., 1997; Hoell et al., 1997; Liu et al., 1999; Pochanart et al., 2001; Jacobson, 2001; Kondo et al., 2004). Large APDM values of up to 10% are simulated in MAM over Southeast Asia because of variations in biomass burning emissions alone (AEMISB–AEMIS). Meanwhile, the IAVs of O<sub>3</sub> are also influenced by biomass burning emissions over Guangxi and Guizhou provinces, with enhanced APDM values of 2–3% (AEMISB–AEMIS) due to the long-range transport of biomass burning from Southeast Asia.

The pressure–latitude plots of the IAVs of O<sub>3</sub> from simulations CTRL, MET, AEMIS, and AEMISB are also shown in Figures 6 and 7 along the longitude of 115°E. The MAD values from the CTRL and MET simulations are larger in the upper troposphere than in the lower troposphere because of the fluxes from the stratosphere to

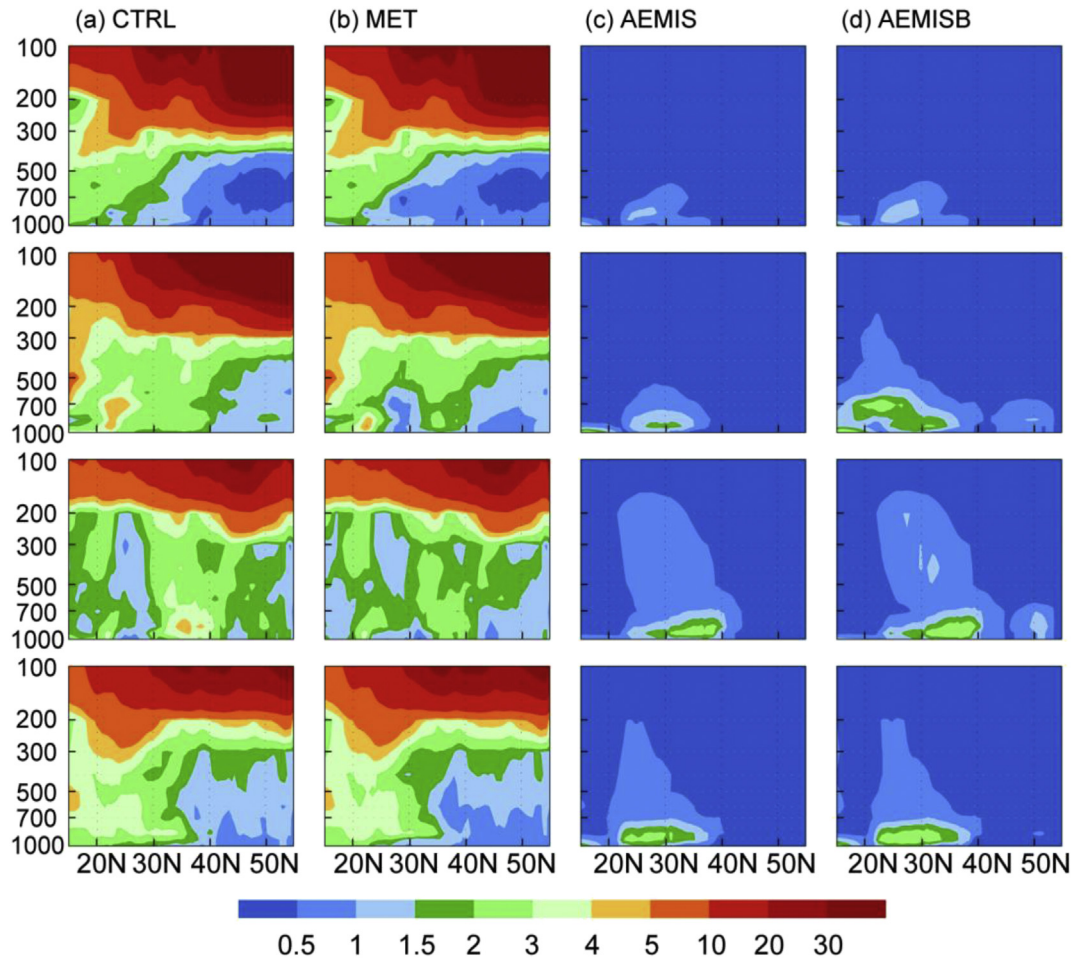


**Fig. 6.** Mean absolute deviation (MAD, ppbv) of O<sub>3</sub> concentrations at the longitudinal plane along 115°E from 15°N to 55°N from simulations of (a) CTRL, (b) MET, (c) AEMIS, and (d) AEMISB for 2004–2012. The vertical axis is atmospheric pressure in hPa.

the troposphere (Sahu et al., 2014; Neu et al., 2014). In the lower and middle troposphere (1000–500 hPa), the IAVs of O<sub>3</sub> are larger over SC than over NC; the APDM values are in the range of 2–10% in all seasons over SC (22–32°N), and are 3–7% in JJA and 1–5% in other three seasons over NC (32–42°N). Such high IAVs in O<sub>3</sub> in the lower and middle troposphere in SC can be attributed to the high IAVs in O<sub>3</sub> transport, which will be discussed in detail in Section 4. The pattern of IAVs of O<sub>3</sub> from the MET simulation is similar to that from the CTRL simulation (Fig. 7 (a) and 7(b)), indicating that the variations in meteorological fields dominate the IAVs of O<sub>3</sub>. The variations in anthropogenic emissions alone (Fig. 7c) can contribute to the IAVs of O<sub>3</sub> in the lower troposphere, with the largest MAD (APDM) values of up to 3 ppbv (4%) over eastern China in both JJA and SON. Comparisons of the IAVs from AEMIS simulation with those from AEMISB simulation indicate that the variations in biomass burning emissions mainly contribute to the IAVs of O<sub>3</sub> in MAM over SC, with MAD (APDM) values of up to 3 ppbv (5%), as a result of the long-range transport of biomass burning emissions from Southeast Asia.

#### 4. Understanding the impacts of variations in meteorological parameters on the IAVs of O<sub>3</sub> by process analyses

##### 4.1. The IAVs of meteorological parameters

Over some specific years, anthropogenic emissions of a species

tend to have a consistent trend of increasing or decreasing, but the IAVs of meteorological parameters can be complex because the IAVs in meteorological fields are mainly associated with the natural variability of climate system. Figure 8 shows the regionally and seasonally averaged winds at 850 hPa, daily maximum temperature, and specific humidity over NC, SC, and SCB for years 2004–2012. The seasonally shifting winds in NC and SC were associated with the East Asian Monsoon. NC was dominated by strong northwesterlies in DJF during the East Asian winter monsoon (EAWM) and by southerlies in JJA during the East Asian summer monsoon (EASM). SC had very strong southerlies in JJA associated with the EASM. Over the SCB, southeasterlies prevailed throughout the year. The seasonal mean winds exhibited large IAVs (Fig. 8a) (Chen et al., 2000; Wu and Wang, 2002), which may lead to large IAVs in the transport of O<sub>3</sub>.

The IAVs of daily max temperature were the largest in DJF in all the regions (NC, SC, and SCB) (Fig. 8b), which agreed with Piao et al. (2003) who showed that temperatures in eastern China had larger IAVs in DJF than in other seasons. The DJF mean of daily max temperature varied over 273.2–278.1, 284.7–288.8, and 280.6–283.6 K over NC, SC, and SCB, respectively, corresponding to MAD values of 1.1–1.2 K in these regions. With respect to specific humidity, the IAVs were larger in JJA than in other seasons over NC and SCB, which varied over the range of 11.2–13.0 and 13.1–14.3 g kg<sup>-1</sup>, respectively. However, the IAV of specific humidity over SC was the largest in DJF, which varied over the range of 4.5–6.1 g kg<sup>-1</sup>.

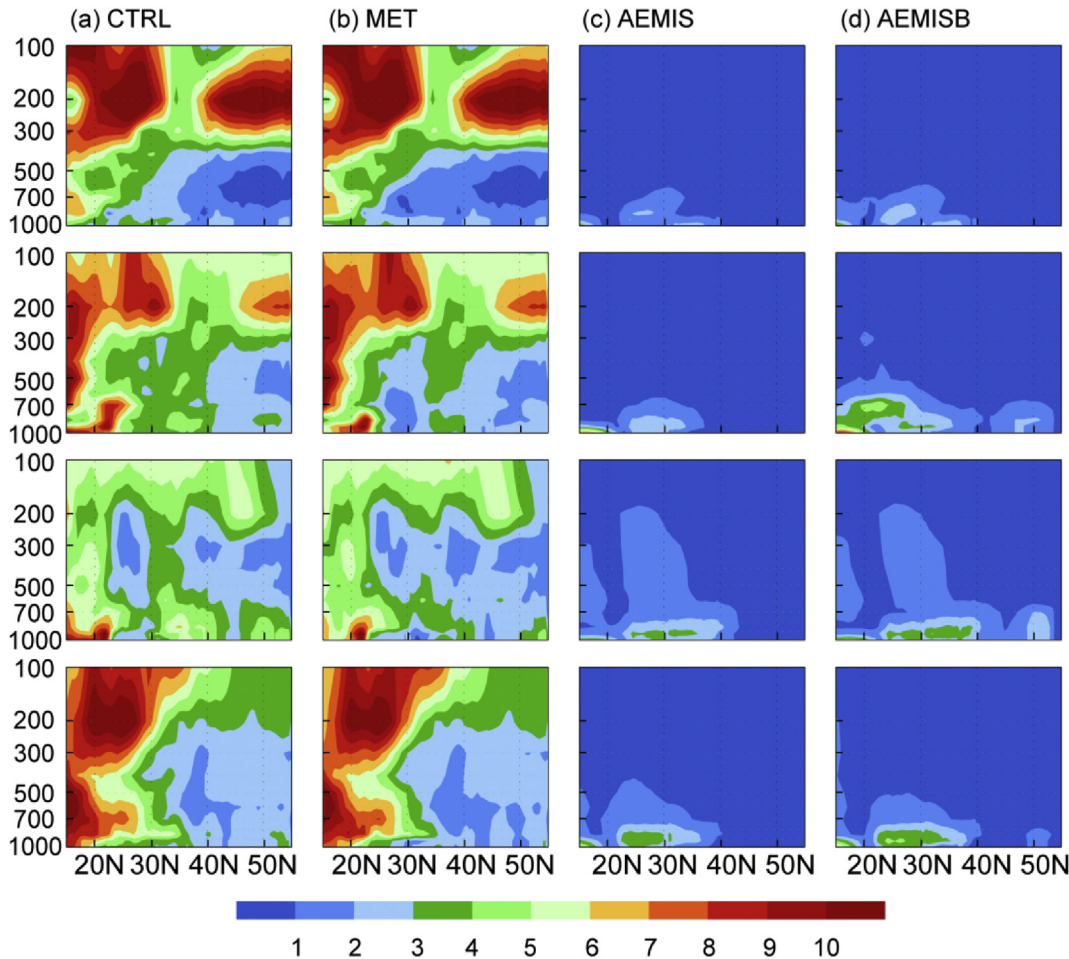


**Fig. 7.** Absolute percent departure from the mean (APDM, %) of  $O_3$  concentrations at the longitudinal plane along 115°E from 15°N to 55°N from simulations of (a) CTRL, (b) MET, (c) AEMIS, and (d) AEMISB for years 2004–2012. The vertical axis is atmospheric pressure in hPa.

#### 4.2. Process analyses

The concentrations of  $O_3$  are determined by precursor emissions, chemical production, chemical loss, transport, and deposition. Therefore, the IAV of each of these processes can influence the IAVs of  $O_3$ . We follow Im et al. (2011) to quantify the contribution of each process to IAVs of  $O_3$  by  $\%PC_i = MAD_i / \sum_i^n MAD_i$ , where  $n$  is the number of processes considered,  $MAD_i$  represents the MAD value of individual process  $i$ , and  $\%PC_i$  is the relative contribution of individual process  $i$  to the total contributions from all processes. Once the dominant processes are selected, meteorological parameters to which the processes are sensitive to are classified as the major meteorological variables that lead to the IAVs of  $O_3$ . Since we aim to quantify the IAVs in surface  $O_3$  concentrations due to variations in meteorological parameters, our process analyses are performed for each of the polluted regions (NC, SC, or SCB) from the surface to 850 hPa on the basis of MET simulation. The budget of  $O_3$  is constructed for the selected region considering the mass balance, including mass flux by transport, dry deposition, chemical production and loss, which are diagnosed at every time step and summed over each season. Note that we do not consider wet deposition of  $O_3$  and meteorology-sensitive biogenic emissions in our process analyses. Wet deposition is not a major process that influences  $O_3$  concentrations (Mickley et al., 1999; Liao et al., 2006). The impacts of meteorology-sensitive biogenic emissions of volatile organic compounds (BVOCs) on the IAVs of  $O_3$  have been found to

be small in Fu and Liao (2012). Over 2001–2006, a maximum APDM of 2% in surface-layer  $O_3$  was simulated in July in southwestern China with variations in BVOC emissions alone, which was much smaller than the APDM value of about 7.5% in July  $O_3$  in the same region simulated with variations in meteorological fields alone (Fu and Liao, 2012).

Figure 9 shows  $O_3$  budget, MAD values and relative contributions of individual processes that influence the IAVs of  $O_3$  for different seasons in NC, SC, and SCB. Transport flux is calculated as the net income flux through the four horizontal boundaries (east, west, south, and north boundaries) and the upper boundary at 850 hPa, while dry deposition,  $O_3$  production and loss are the sums over the grid cells of the region from surface to 850 hPa. Over NC, chemical production of  $O_3$  has the largest value among the processes that influence  $O_3$  budget in all seasons (Fig. 9a). With strong photochemistry in JJA, the chemical production in NC reaches 11.0 Tg season<sup>-1</sup>. However, chemical production of  $O_3$  has smaller IAV than transport flux, as indicated by the smaller MAD values in Figure 9d. As a result, chemical production has relative contributions 28–34% in all seasons, which are significant but smaller than the relative contributions from transport flux of  $O_3$ . Although the absolute values of transport flux are small, the large MAD values of transport flux lead to high relative contributions of 46–52%, indicating that transport is the most important process that influences the IAVs of  $O_3$ . Dry deposition and chemical loss of  $O_3$  have small impacts on the IAVs of  $O_3$ , with relative contributions less than 13%

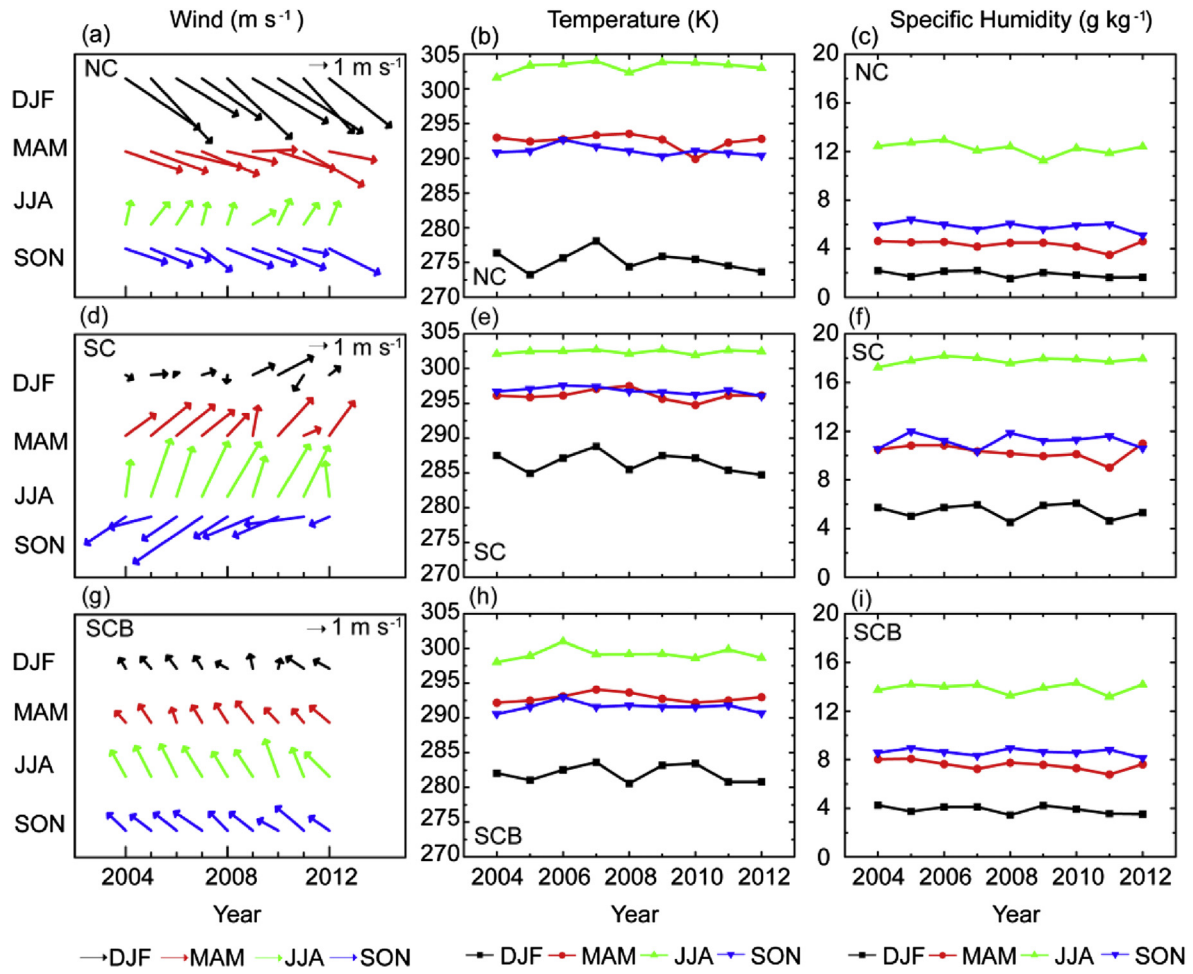


**Fig. 8.** Yearly variations in winds at 850 hPa ( $\text{m s}^{-1}$ ), daily max temperature (K), and specific humidity ( $\text{g kg}^{-1}$ ) that are averaged over NC, SC, and SCB.

throughout the year. Over NC, transport and chemical production of  $\text{O}_3$  have a total relative contribution of exceeding 78% in all seasons. Since the transport flux is sensitive to winds, and  $\text{O}_3$  production is sensitive to temperature and humidity (Camalier et al., 2007; Vieno et al., 2010; Ramsey et al., 2014), we conclude that the variations in winds are the major factors that determine the IAVs of  $\text{O}_3$  over NC, followed by those in temperature and humidity. Note that the relative contribution of chemical production of  $\text{O}_3$  is the largest (34%) in DJF (Fig. 9g), which is supported by the largest variations in daily maximum temperature in DJF over NC (Fig. 8).

Similar analyses are carried out for  $\text{O}_3$  in SC. The transport mass flux over SC has the maximum relative contributions of 59–63%, corresponding well with the large IAVs of regional wind over SC (Fig. 8). Chemical production of  $\text{O}_3$  is again the second largest contributor to the IAVs of  $\text{O}_3$ , with relative contributions of 16–21% throughout the year. In MAM and JJA in SC, chemical loss has relative contributions of about 15%, which are the highest among all regions, reflecting the role of highest specific humidity in SC (Fig. 8).

With respect to  $\text{O}_3$  budget over the SCB, transport is the most important process that contributes to the IAVs of  $\text{O}_3$ , with relative contributions of 58–87% throughout the year. The other processes show much smaller contributions compare to transport. In JJA when photochemistry is the strongest in SCB,  $\text{O}_3$  production and loss have relative contributions of 22% and 14%, respectively.

## 5. Impacts of $\text{O}_3$ flux from the stratosphere to the troposphere on the IAVs of $\text{O}_3$

As reviewed in our introduction section, the flux of  $\text{O}_3$  from the stratosphere to troposphere (STE) can influence the IAVs of tropospheric  $\text{O}_3$  concentrations. We quantify here the impact of STE on the IAVs of  $\text{O}_3$  in China by comparisons of model results between TROP and MET simulations (see Section 2.3 for description of simulations). The variations in STE flux (MET–TROP) are simulated to lead to small MAD values of less than 0.4 ppbv in seasonal mean surface-layer  $\text{O}_3$  over China in all seasons (not shown), and to lead to APDM values of 1–2% in  $\text{O}_3$  concentrations in the middle-to-upper troposphere over  $30^{\circ}$ – $50^{\circ}$  N. Our results are supported by those in Lin et al. (2014) and Neu et al. (2014). Lin et al. (2014) found that the impact of the STE flux on the IAVs of free tropospheric  $\text{O}_3$  at Mauna Loa Observatory (with an altitude of 3.4 km) was much smaller than the impacts of long-range transport from Asia, on the basis of 40-year observations and simulations with the Geophysical Fluid Dynamic Laboratory global chemistry-climate model (GFDL AM3) model. Neu et al. (2014) reported a 2% change in 500 hPa  $\text{O}_3$  averaged over  $30^{\circ}$ – $50^{\circ}$  N due to the IAVs in STE.

## 6. Conclusions

We use the global 3-D chemical transport model GEOS-Chem to quantify the roles of meteorology, anthropogenic emissions, and biomass burning emissions in the IAVs of  $\text{O}_3$  over China from 2004

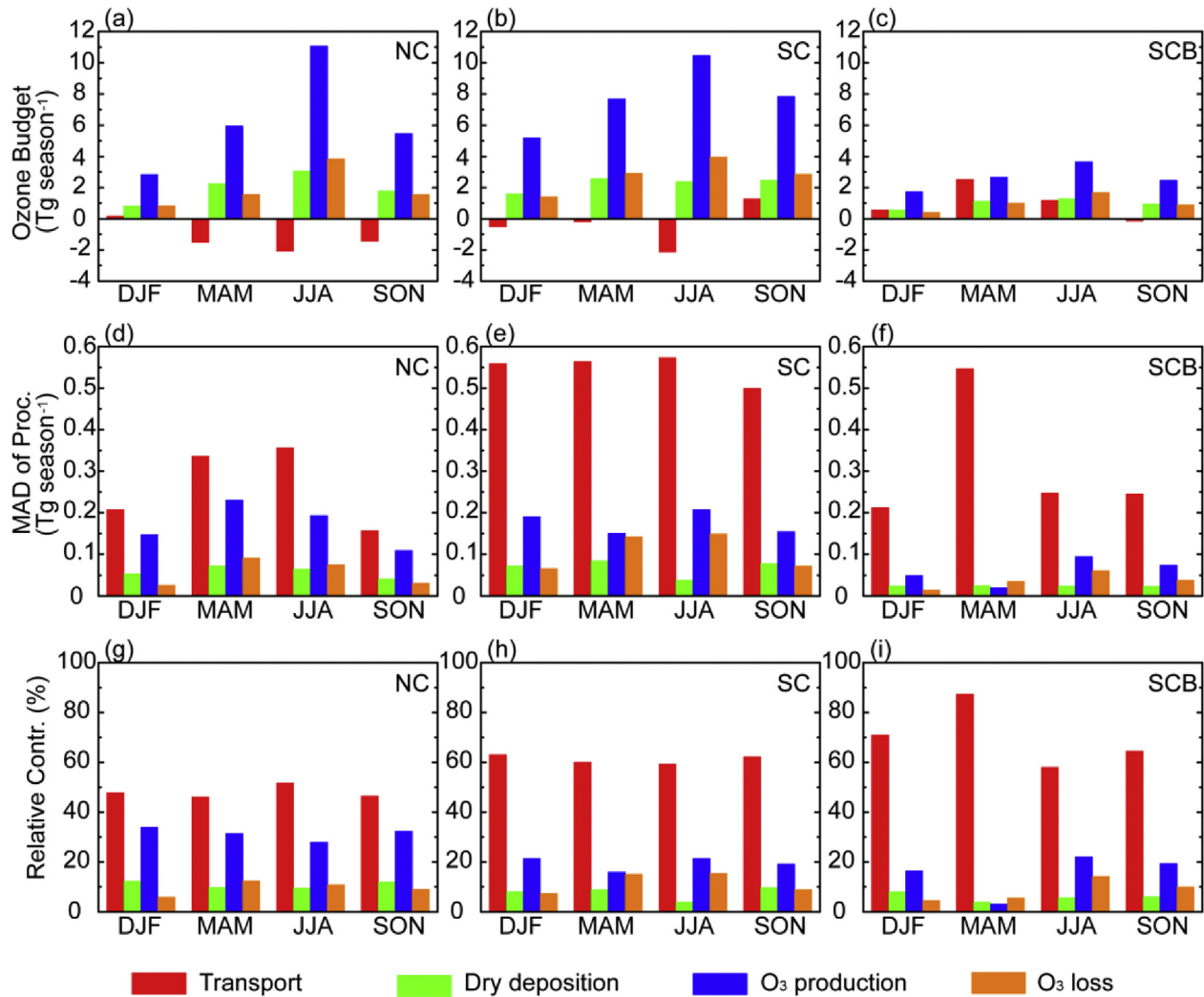


**Fig. 9.** O<sub>3</sub> budget ( $\text{Tg season}^{-1}$ ), MAD values ( $\text{Tg season}^{-1}$ ) and relative contributions (%) of individual processes (transport, dry deposition, chemical production and loss) that influence the IAVs of O<sub>3</sub> for different seasons in NC, SC, and SCB. Transport flux is calculated as the net income flux through the four horizontal boundaries and the upper boundary at 850 hPa, while dry deposition, O<sub>3</sub> production and loss are the sums over the grid cells of the region under 850 hPa.

to 2012. We have performed simulations CTRL (the combined effects of variations in meteorological parameters and anthropogenic emissions), MET (effects of variations in meteorological parameters alone), AEMIS (effects of variations in anthropogenic emissions alone), and AEMISB (effects of variations in both anthropogenic and biomass burning emissions) to identify the key factors that influence the IAVs of O<sub>3</sub>.

We use two statistical parameters, mean absolute deviation (MAD) and absolute percent departure from the mean (APDM), to quantify the IAVs of O<sub>3</sub> concentrations for years 2004–2012. Driven by variations in both meteorology and emissions (anthropogenic plus biomass burning emissions), the regional mean APDM values of seasonal mean surface-layer O<sub>3</sub> simulated in the CTRL simulation are in the range of 0.7–3.9%, 1.4–3.7%, and 2.7–3.8%, respectively, over NC, SC, and SCB. Over NC, the IAVs in surface-layer O<sub>3</sub> by variations in meteorological fields are larger than those by variations in anthropogenic emissions throughout the year; the APDM values of O<sub>3</sub> are in the range of 1.2–2.6% in MET simulation and 0.6–1.9% in AEMIS simulation. Over SC, compared to the IAVs in O<sub>3</sub> resulted from the variations in emissions (AEMIS), the IAVs of O<sub>3</sub> owing to variations in meteorological fields (MET) are larger in DJF, MAM, and SON whereas smaller in JJA. The relatively more

important role of variations in anthropogenic emissions is also simulated in SCB in all seasons. Note that the variations in biomass burning emissions alone (AEMISB–AEMIS) lead to enhanced APDM values of 2–3% in surface-layer O<sub>3</sub> concentrations over Guangxi and Guizhou provinces in MAM, because of the long-range transport of biomass burning emissions from southeast Asia. The significance of these IAVs of O<sub>3</sub> can be demonstrated when they are compared with the changes in O<sub>3</sub> concentrations driven by reductions in emissions. Studies showed that summer O<sub>3</sub> concentrations over eastern China varied by 10–20% as a result of the 50% reductions in NO<sub>x</sub> or VOCs (anthropogenic plus biogenic VOCs) (Han et al., 2005).

We have performed process analyses to identify key meteorological parameters that influence the IAVs of O<sub>3</sub>. Over NC and SC, transport flux and chemical production are found to be the first and second important processes that drive the IAVs of O<sub>3</sub> throughout the year, with relative contributions of, respectively, 46–52% and 28–34% over NC and 59–63% and 16–21% in SC. Over SCB, transport is the most dominant process that leads to the IAVs of O<sub>3</sub>, with high relative contributions of 58–87% throughout the year. Therefore, variations in winds have the largest impact on the IAVs of O<sub>3</sub> over the three polluted regions, followed by variations in temperature and specific humidity.

The IAVs in meteorological fields are mainly associated with natural variability in the climate system; hence the magnitudes of IAVs in O<sub>3</sub> concentrations driven by meteorological parameters have important implications for the effectiveness of short-term air quality control strategies in China. For example, we have found that the IAVs of O<sub>3</sub> caused by variations in meteorological parameters are larger than those caused by variations in emissions in NC and SC, indicating that the short-term air quality control in NC and SC need extra efforts to reduce emissions if the meteorological parameters are not favorable to O<sub>3</sub> air quality. It should be noted that, for studies on longer timescales, the MAD and APDM values need to be calculated after detrending the time series, following the approach used in previous studies that examined IAVs of O<sub>3</sub> in the tropics (Camp et al., 2003).

Comparisons of our model results with very limited ground-based measurements at Tap Mum, Waliguan, Everest-Pyramid, and Ryori indicate that the IAVs of O<sub>3</sub> simulated in our model are smaller than those obtained from the measurements. The model might have underestimated high O<sub>3</sub> values and overestimated low observed values on interannual time scale, which suggests further improvements in studies of IAVs of O<sub>3</sub>. Emission inventories of O<sub>3</sub> precursors, aerosol precursors, and aerosols need continuing improvement in terms of both total amount and interannual variations. Furthermore, nationwide long-term ground-based measurements of tropospheric O<sub>3</sub> are needed for evaluation of simulated IAVs.

## Acknowledgments

This work was supported by the National Basic Research Program of China (973 program, Grant 2014CB441202) and the Strategic Priority Research Program of the Chinese Academy of Sciences (Grant No. XDA05100503). We also acknowledge the WMO-World Data Centre for Greenhouse Gases for providing the measurements of O<sub>3</sub>.

## References

- Alexander, B., Park, R.J., Jacob, D.J., Li, Q.B., Yantosca, R.M., Savarino, J., Lee, C.C.W., Thiemens, M.H., 2005. Sulfate formation in sea-salt aerosols: constraints from oxygen isotopes. *J. Geophys. Res.* 110, D10307. <http://dx.doi.org/10.1029/2004jd005659>.
- Bey, I., Jacob, D.J., Yantosca, R.M., Logan, J.A., Field, B., Fiore, A.M., Li, Q., Liu, H., Mickley, L.J., Schultz, M., 2001. Global modeling of tropospheric chemistry with assimilated meteorology: model description and evaluation. *J. Geophys. Res.* 106, 23,073–23,095. <http://dx.doi.org/10.1029/2001JD000807>.
- Camalier, L., Cox, W., Dolwick, P., 2007. The effects of meteorology on ozone in urban areas and their use in assessing ozone trends. *Atmos. Environ.* 7127–7137. <http://dx.doi.org/10.1016/j.atmosenv.2007.04.061>.
- Camp, C.D., Roulston, M.S., Yung, Y.L., 2003. Temporal and spatial patterns of the interannual variability of total ozone in the tropics. *J. Geophys. Res.* 108 (D20), 4643. <http://dx.doi.org/10.1029/2001JD001504>.
- Chatani, S., Sudo, K., 2011. Influences of the variation in inflow to East Asia on surface ozone over Japan during 1996–2005. *Atmos. Chem. Phys.* 11, 8745–8758. <http://dx.doi.org/10.5194/acp-11-8745-2011>.
- Chen, D., Wang, Y.X., McElroy, M.B., He, K., Yantosca, R.M., Le Sager, P., 2009. Regional CO pollution in China simulated by the high-resolution nested-grid GEOS-Chem model. *Atmos. Chem. Phys.* 9, 3825–3839. <http://dx.doi.org/10.5194/acp-9-3825-2009>.
- Chen, W., Graf, H., Huang, R., 2000. The interannual variability of East Asian winter monsoon and its relation to the summer monsoon. *Adv. Atmos. Sci.* 17 (1), 48–60. <http://dx.doi.org/10.1007/s00376-000-0042-5>.
- Civerolo, K., Hogrefe, C., Zalewsky, E., Hao, W., Sistla, G., Lynn, B., Rosenzweig, C., Kinney, P.L., 2010. Evaluation of an 18-year CMAQ simulation: seasonal variations and long-term temporal changes in sulfate and nitrate. *Atmos. Environ.* 44, 3745–3752. <http://dx.doi.org/10.1016/j.atmosenv.2010.06.056>.
- Dawson, J.P., Adams, P.J., Pandis, S.N., 2007. Sensitivity of ozone to summertime climate in the eastern USA: a modeling case study. *Atmos. Environ.* 41, 1494–1511. <http://dx.doi.org/10.1015/j.atmosenv.2006.10.033>.
- Ding, A., Wang, T., 2006. Influence of stratosphere-to-troposphere exchange on the seasonal cycle of surface ozone at Mount Waliguan in western China. *Geophys. Res. Lett.* 33, L03803. <http://dx.doi.org/10.1029/2005GL024760>.
- Duan, J.C., Tan, J.H., Yang, L., Wu, S., Hao, J.M., 2008. Concentration, sources and ozone formation potential of volatile organic compounds (VOCs) during ozone episode in Beijing. *Atmos. Res.* 88, 25–35. <http://dx.doi.org/10.1016/j.atmosres.2007.09.004>.
- Fairlie, T.D., Jacob, D.J., Park, R.J., 2007. The impact of transpacific transport of mineral dust in the United States. *Atmos. Environ.* 41, 1251–1266. <http://dx.doi.org/10.1016/j.atmosenv.2006.09.048>.
- Fu, J.S., Hsu, N.C., Gao, Y., Huang, K., Li, C., Lin, N.-H., Tsay, S.-C., 2012. Evaluating the influences of biomass burning during 2006 BASE-ASIA: a regional chemical transport modeling. *Atmos. Chem. Phys.* 12, 3837–3855. <http://dx.doi.org/10.5194/acp-12-3837-2012>.
- Fu, Y., Liao, H., 2012. Simulation of the interannual variations of biogenic emissions of volatile organic compounds in China: impacts on tropospheric ozone and secondary organic aerosol. *Atmos. Environ.* 59, 170–185. <http://dx.doi.org/10.1016/j.atmosenv.2012.05.053>.
- Ge, B.Z., Xu, X.B., Lin, W.L., Li, J., Wang, Z.F., 2012. Impact of the regional transport of urban Beijing pollutants on downwind areas in summer: ozone production efficiency analysis. *Tellus B* 64, 17348. <http://dx.doi.org/10.3402/tellusb.v6410.17348>.
- Goncalves, M., Jimenez-Guerrero, P., Baldasano, J.M., 2009. Contribution of atmospheric processes affecting the dynamics of air pollution in South-Western Europe during a typical summertime photochemical episode. *Atmos. Chem. Phys.* 9, 849–864. <http://dx.doi.org/10.5194/acp-9-849-2009>.
- Guenther, A.B., Jiang, X., Heald, C.L., Sakulyanontvittaya, T., Duhl, T., Emmons, L.K., Wang, X., 2012. The model of emissions of gases and aerosols from nature version 2.1 (MEGAN2.1): an extended and updated framework for modeling biogenic emissions. *Geosci. Model Dev.* 5, 1471–1492. <http://dx.doi.org/10.5194/gmd-5-1471-2012>.
- Han, Z., Ueda, H., Matsuda, K., 2005. Model study of the impact of biogenic emission on regional ozone and the effectiveness of emission reduction scenarios over eastern China. *Tellus* 57, 12–27. <http://dx.doi.org/10.1111/j.1600-0889.2005.00132.x>.
- Hess, P.G., Zbinden, R., 2013. Stratospheric impact on tropospheric ozone variability and trends: 1990–2009. *Atmos. Chem. Phys.* 13, 649–674. <http://dx.doi.org/10.5194/acp-13-649-2013>.
- Hoell, J.M., Davis, D.D., Liu, S.C., Newell, R.E., Akimoto, H., Bendura, R.J., 1997. The pacific exploratory mission-west phase B: February–March 1994. *J. Geophys. Res.* 102, 28,223–28,239. <http://dx.doi.org/10.1029/97JD02581>.
- Hogrefe, C., Hao, W., Zalewsky, E.E., Ku, J.-Y., Lynn, B., Rosenzweig, C., Schultz, M.G., Rast, S., Newchurch, M.J., Wang, L., Kinney, P.L., Sistla, G., 2011. An analysis of long-term regional-scale ozone simulations over the Northeastern United States: variability and trends. *Atmos. Chem. Phys.* 11, 567–582. <http://dx.doi.org/10.5194/acp-11-567-2011>.
- Im, U., Markakis, K., Poupkou, A., Melas, D., Unal, A., Gerasopoulos, E., Daskalakis, N., Kindap, T., Kanakidou, M., 2011. The impact of temperature changes on summer time ozone and its precursors in the Eastern Mediterranean. *Atmos. Chem. Phys.* 11, 3847–3864. <http://dx.doi.org/10.5194/acp-11-3847-2011>.
- IPCC, 2013. Climate change 2013: the physical science basis. In: Stocker, T.F., et al. (Eds.), *Contribution of Working Group I to the Fifth Assessment Report of the Intergovernmental Panel on Climate Change*. Cambridge University Press, Cambridge, United Kingdom and New York, 1–1535.
- Jacobson, M.Z., 2001. Strong radiative heating due to the mixing state of black carbon in atmospheric aerosols. *Nature* 409, 695–697. <http://dx.doi.org/10.1038/35055518>.
- Jiang, X.Y., Wiedinmyer, C., Chen, F., Yang, Z.-L., Lo, J.-C.-F., 2008. Predicted impacts of climate and land use change on surface ozone in the Houston, Texas, area. *J. Geophys. Res.* 113, D20312. <http://dx.doi.org/10.1029/2008JD009820>.
- Jiang, F., Zhou, P., Liu, Q., Wang, T.J., Zhuang, B.L., Wang, X.Y., 2012. Modeling tropospheric ozone formation over East China in springtime. *J. Atmos. Chem.* 69, 303–319. <http://dx.doi.org/10.1007/s10874-012-9244-3>.
- Jiang, Z., Liu, Z., Wang, T., Schwartz, C.S., Lin, H.-C., Jiang, F., 2013. Probing into the impact of 3DVAR assimilation of surface PM10 observations over China using process analysis. *J. Geophys. Res.* 118, 6738–6749. <http://dx.doi.org/10.1002/jgrd.50495>.
- Jose, R.S., Perez, J.L., Pleguezuelos, C., Camacho, F., Gonzalez, R.M., 2002. MM5-CMAQ air quality modeling process analysis: Madrid case. *Adv. Air Pollut. Ser.* 11, 171–179.
- Kondo, Y., Morino, Y., Takegawa, N., Koike, M., Kita, K., Miyazaki, Y., Sachse, G.W., Vay, S.A., Avery, M.A., Flocke, F., Weinheimer, A.J., Eisele, F.L., Zondlo, M.A., Weber, R.J., Singh, H.B., Chen, G., Crawford, J., Blake, D.R., Fuelberg, H.E., Clarke, A.D., Talbot, R.W., Sandholm, S.T., Browell, E.V., Streets, D.G., 2004. Impacts of biomass burning in Southeast Asia on ozone and reactive nitrogen over the western Pacific in spring. *J. Geophys. Res.* 109, D15S12. <http://dx.doi.org/10.1029/2003JD004203>.
- Kumar, A., Wu, S., Weise, M.F., Honrath, R., Owen, R.C., Helmig, D., Kramer, L., Val Martin, M., Li, Q., 2013. Free-troposphere ozone and carbon monoxide over the North Atlantic for 2001–2011. *Atmos. Chem. Phys.* 13, 12537–12547. <http://dx.doi.org/10.5194/acp-13-12537-2013>.
- Li, J., Wang, Z., Akimoto, H., Tang, J., Uno, I., 2009. Modeling of the impacts of China's anthropogenic pollutants on the surface ozone summer maximum on the northern Tibetan Plateau. *Geophys. Res. Lett.* 36, L24802. <http://dx.doi.org/10.1029/2009GL041123>.
- Liao, H., Chen, W.-T., Seinfeld, J.H., 2006. Role of climate change in global predictions of future tropospheric ozone and aerosols. *J. Geophys. Res.* 111, D12304. <http://dx.doi.org/10.1029/2005JD006852>.
- Lin, C.-Y.C., Jacob, D.J., Fiore, A.M., 2001. Trends in exceedances of the ozone air

- quality standard in the continental United States, 1980–1998. *Atmos. Environ.* 35, 3217–3228. [http://dx.doi.org/10.1016/S1352-2310\(01\)00152-2](http://dx.doi.org/10.1016/S1352-2310(01)00152-2).
- Lin, M., Horowitz, L.W., Oltmans, S.J., Fiore, A.M., Fan, S., 2014. Tropospheric ozone trends at Mauna Loa observatory tied to decadal climate variability. *Nat. Geosci.* 7, 136–143. <http://dx.doi.org/10.1038/ngeo2066>.
- Liu, H.Y., Chang, W.L., Oltmans, S.J., 1999. On springtime high ozone events in the lower troposphere from Southeast Asian biomass burning. *Atmos. Environ.* 33 (11), 2403–2410. [http://dx.doi.org/10.1016/S1352-2310\(98\)00357-4](http://dx.doi.org/10.1016/S1352-2310(98)00357-4).
- Liu, J.J., Jones, D.B.A., Zhang, S., Kar, J., 2011. Influence of interannual variations in transport on summertime abundances of ozone over the middle East. *J. Geophys. Res.* 116, D20310. <http://dx.doi.org/10.1029/2011JD016188>.
- Liu, X., Chance, K., Sioris, C.E., Kurosawa, T.P., Spurr, R.J.D., Martin, R.V., Fu, T., Logan, J.A., Jacob, D.J., Palmer, P.I., Newchurch, M.J., Megretskia, I.A., Chatfield, R.B., 2006. First directly retrieved global distribution of tropospheric column ozone from GOME: comparison with the GEOS-CHEM model. *J. Geophys. Res.* 111, D02308. <http://dx.doi.org/10.1029/2005JD006564>.
- Lou, S., Liao, H., Zhu, B., 2014. Impacts of aerosols on surface-layer ozone concentrations in China through heterogeneous reactions and changes in photolysis rates. *Atmos. Environ.* 85, 123–138. <http://dx.doi.org/10.1016/j.atmosenv.2013.12.004>.
- Mu, Q., Liao, H., 2014. Simulation of the interannual variations of aerosols in China: role of variations in meteorological parameters. *Atmos. Chem. Phys.* 14, 9597–9612. <http://dx.doi.org/10.5194/acp-14-9597-2014>.
- McLinden, C.A., Olsen, S.C., Hannegan, B., Wild, O., Prather, M.J., Sunder, J., 2000. Stratospheric ozone in 3-D models: a simple chemistry and the cross-tropopause flux. *J. Geophys. Res.* 105, 14653–14665. <http://dx.doi.org/10.1029/2000JD900124>.
- Mickley, L.J., Murti, P.P., Jacob, D.J., Logan, J.A., Koch, D.M., Rind, D., 1999. Radiative forcing from tropospheric ozone calculated with a unified chemistry-climate model. *J. Geophys. Res.* 104, 30,153–30,172. <http://dx.doi.org/10.1029/1999JD900439>.
- Murray, L.T., Jacob, D.J., Logan, J.A., Hudman, R.C., Koshak, W.J., 2012. Optimized regional and interannual variability of lightning in a global chemical transport model constrained by LIS/OTD satellite data. *J. Geophys. Res.* 117, D20307. <http://dx.doi.org/10.1029/2012JD017934>.
- Neu, J.L., Flury, T., Manney, G.L., Santee, M.L., Livesey, N.J., Worden, J., 2014. Tropospheric ozone variations governed by changes in stratospheric circulation. *Nat. Geosci.* 7, 340–344. <http://dx.doi.org/10.1038/ngeo2138>.
- Newell, R.E., Browell, E.V., Davis, D.D., Liu, S.C., 1997. Western Pacific tropospheric ozone and potential vorticity: implications for Asian pollution. *Geophys. Res. Lett.* 24, 2733–2736. <http://dx.doi.org/10.1029/97GL02799>.
- Olsen, M.A., Douglass, A.R., Kaplan, T.B., 2013. Variability of extratropical ozone stratosphere–troposphere exchange using microwave limb sounder observations. *J. Geophys. Res.* 118, 1090–1099. <http://dx.doi.org/10.1029/2012JD018465>.
- Park, R.J., Jacob, D.J., Chin, M., Martin, R.V., 2003. Sources of carbonaceous aerosols over the United States and implications for natural visibility. *J. Geophys. Res.* 108 (D12), 4355. <http://dx.doi.org/10.1029/2002JD003190>.
- Park, R.J., Jacob, D.J., Field, B.D., Yantosca, R.M., Chin, M., 2004. Natural and trans-boundary pollution influences on sulfate–nitrate–ammonium aerosols in the United States: implications for policy. *J. Geophys. Res.* 109, D15204. <http://dx.doi.org/10.1029/2003JD004473>.
- Piao, S.L., Fang, J.Y., Zhou, L.M., Guo, Q.H., Henderson, M., Ji, W., Li, Y., Tao, S., 2003. Interannual variations of monthly and seasonal normalized difference vegetation index (NDVI) in China from 1982 to 1999. *J. Geophys. Res.* 108, 4401. <http://dx.doi.org/10.1029/2002jd002848>.
- Pochanart, P., Kreasuwun, J., Sukasem, P., Geerathithadaniyom, W., Tabucanon, M.S., Hirokawa, J., Kajii, Y., Akimoto, H., 2001. Tropical tropospheric ozone observed in Thailand. *Atmos. Environ.* 35, 2657–2668. [http://dx.doi.org/10.1016/S1352-2310\(00\)0441-6](http://dx.doi.org/10.1016/S1352-2310(00)0441-6).
- Pozzoli, L., Janssens-Maenhout, G., Diehl, T., Bey, I., Schultz, M.G., Feichter, J., Vignati, E., Dentener, F., 2011. Re-analysis of tropospheric sulfate aerosol and ozone for the period 1980–2005 using the aerosol-chemistry-climate model ECHAM5-HAMMOZ. *Atmos. Chem. Phys.* 11, 9563–9594. <http://dx.doi.org/10.5194/acp-11-9563-2011>.
- Pye, H.O.T., Liao, H., Wu, S., Mickley, L.J., Jacob, D.J., Henze, D.K., Seinfeld, J.H., 2009. Effect of changes in climate and emissions on future sulfate–nitrate–ammonium aerosol levels in the United States. *J. Geophys. Res.* 114, D01205. <http://dx.doi.org/10.1029/2008jd010701>.
- Ramsey, N.R., Klein, P.M., Moore III, B., 2014. The impact of meteorological parameters on urban air quality. *Atmos. Environ.* 86, 58–67. <http://dx.doi.org/10.1016/j.atmosenv.2013.12.006>.
- Sahu, L.K., Sheel, V., Kajino, M., Deushi, M., Gunthe, S.S., Sinha, P.R., Sauvage, B., Thouret, V., Smit, H.G., 2014. Seasonal and interannual variability of tropospheric ozone over an urban site in India: a study based on MOZAIC and CCM vertical profiles over Hyderabad. *J. Geophys. Res.* 119, 3615–3641. <http://dx.doi.org/10.1002/2013JD021215>.
- Sauvage, B., Martin, R.V., van Donkelaar, A., Liu, X., Chance, K., Jaegle, L., Palmer, P.I., Wu, S., Fu, T.-M., 2007. Remote sensed and in situ constraints on processes affecting tropical tropospheric ozone. *Atmos. Chem. Phys.* 7, 815–838. <http://dx.doi.org/10.5194/acp-7-815-2007>.
- Sekiya, T., Sudo, K., 2014. Roles of transport and chemistry processes in global ozone change on interannual and multidecadal time scales. *J. Geophys. Res.* 119, 4903–4921. <http://dx.doi.org/10.1002/2013JD020838>.
- Shindell, D., Kylenstierna, J.C.I., Vignati, E., van Dingenen, R., Amann, M., Klimont, Z., Anenberg, S.C., Muller, N., Janssens-Maenhout, G., Raes, F., Schwartz, J., Faluvegi, G., Pozzoli, L., Kupiainen, K., Höglund-Isaksson, L., Emberson, L., Streets, D., Ramanathan, V., Hicks, K., Oanh, N.T.K., Millly, G., Williams, M., Demkine, V., Fowler, D., 2012. Simultaneously mitigating near-term climate change and improving human health and food security. *Science* 335, 183–189. <http://dx.doi.org/10.1126/science.1210026>.
- Tang, G., Li, X., Wang, Y., Xin, J., Ren, X., 2009. Surface ozone trend details and interpretations in Beijing, 2001–2006. *Atmos. Chem. Phys.* 9, 8813–8823. <http://dx.doi.org/10.5194/acp-9-8813-2009>.
- UNEP, 2006. *Environmental Effects of Ozone Depletion and its Interactions with Climate Change: 2006 Assessment*.
- van der Werf, G.R., Randerson, J.T., Giglio, L., Collatz, G.J., Mu, M., Kasibhatla, P.S., Morton, D.C., DeFries, R.S., Jin, Y., van Leeuwen, T.T., 2010. Global fire emissions and the contribution of deforestation, savanna, forest, agricultural, and peat fires (1997–2009). *Atmos. Chem. Phys.* 10, 11707–11735. <http://dx.doi.org/10.5194/acp-10-11707-2010>.
- Van Donkelaar, A., Martin, R.V., Leitch, W.R., Macdonald, A.M., Walker, T.W., Streets, D.G., Zhang, Q., Dunlea, E.J., Jimenez, J.L., Dibb, J.E., Huey, L.G., Weber, R., Andreae, M.O., 2008. Analysis of aircraft and satellite measurements from the intercontinental chemical transport experiment (INTEX-B) to quantify long-range transport of East Asian sulfur to Canada. *Atmos. Chem. Phys.* 8, 2999–3014. <http://dx.doi.org/10.5194/acp-8-2999-2008>.
- Vieno, M., Dore, A.J., Stevenson, D.S., Doherty, R., Heal, M.R., Reis, S., Hallsworth, S., Tarrason, L., Wind, P., Fowler, D., Simpson, D., Sutton, M.A., 2010. Modelling surface ozone during the 2003 heat-wave in the UK. *Atmos. Chem. Phys.* 10, 7963–7978. <http://dx.doi.org/10.5194/acp-10-7963-2010>.
- Voulgarakis, A., Hadjinicolaou, P., Pyle, J.A., 2011. Increases in global tropospheric ozone following an El Niño event: examining stratospheric ozone variability as a potential driver. *Atmos. Sci. Lett.* 12, 228–232. <http://dx.doi.org/10.1002/asl.318>.
- Wang, T., Ding, A., Gao, J., Wu, W.S., 2006. Strong ozone production in urban plumes from Beijing, China. *Geophys. Res. Lett.* 33, L21806. <http://dx.doi.org/10.1029/2006GL027689>.
- Wang, Y., McElroy, M.B., Munger, J.W., Hao, J., Ma, H., Nielsen, C.P., Chen, Y., 2008. Variations of O<sub>3</sub> and CO in summertime at a rural site near Beijing. *Atmos. Chem. Phys.* 8, 6355–6363. <http://dx.doi.org/10.5194/acp-8-6355-2008>.
- Wang, Y., Zhang, Y., Hao, J., Luo, M., 2011. Seasonal and spatial variability of surface ozone over China: contributions from background and domestic pollution. *Atmos. Chem. Phys.* 11, 3511–3525. <http://dx.doi.org/10.5194/acp-11-3511-2011>.
- Wei, W., Wang, S., Hao, J., Cheng, S., 2014. Trends of chemical speciation profiles of anthropogenic volatile organic compounds emissions in China, 2005–2020. *Front. Environ. Sci. Eng.* 8 (1), 27–41. <http://dx.doi.org/10.1007/s11783-012-0461-4>.
- Wild, O., Akimoto, H., 2001. Intercontinental transport of ozone and its precursors in a three-dimensional global CTM. *J. Geophys. Res.* 106 (D21), 27,729–27,744. <http://dx.doi.org/10.1029/2000JD000123>.
- Wu, B., Wang, J., 2002. Winter Arctic oscillation, Siberian high and East Asian winter monsoon. *Geophys. Res. Lett.* 29 (19), 1897. <http://dx.doi.org/10.1029/2002GL015373>.
- Xu, X., Lin, W., Wang, T., Yan, P., Tang, J., Meng, Z., Wang, Y., 2008. Long-term trend of surface ozone at a regional background station in eastern China 1991–2006: enhanced variability. *Atmos. Chem. Phys.* 8, 2595–2607. <http://dx.doi.org/10.5194/acp-8-2595-2008>.
- Yang, G., Fan, S., Tang, J., Jin, S., Meng, Z., 2008. Characteristic of surface ozone concentrations at Lin'an. *Res. Environ. Sci.* 21 (3), 31–35 (in Chinese).
- Yang, Y., Liao, H., Li, J., 2014. Impacts of the East Asian summer monsoon on interannual variations of summertime surface-layer ozone concentrations over China. *Atmos. Chem. Phys.* 14, 6867–6880. <http://dx.doi.org/10.5194/acp-14-6867-2014>.
- Yienger, J.J., Levy, H., 1995. Empirical model of global soil biogenic NO<sub>x</sub> emissions. *J. Geophys. Res.* 100, 11447–11464. <http://dx.doi.org/10.1029/95JD00370>.
- Yumimoto, K., Uno, I., Itahashi, S., 2014. Long-term inverse modeling of Chinese CO emission from satellite observations. *Environ. Pollut.* 195, 308–318. <http://dx.doi.org/10.1016/j.envpol.2014.07.026>.
- Zhang, Y.H., Hu, M., Zhong, L.J., Widensohler, A., Liu, S.C., Andreae, M.O., Wang, W., Fan, S.J., 2008. Regional integrated experiments on air quality over Pearl River Delta 2004 (PRIDE-PRD2004): overview. *Atmos. Environ.* 42, 6157–6173.
- Zhang, Q., Streets, D.G., Carmichael, G.R., He, K.B., Huo, H., Kannari, A., Klimont, Z., Park, I.S., Reddy, S., Fu, J.S., Chen, D., Duan, L., Lei, Y., Wang, L.T., Yao, Z.L., 2009a. Asian emissions in 2006 for the NASA INTEX-B mission. *Atmos. Chem. Phys.* 9, 5131–5153. <http://dx.doi.org/10.5194/acp-9-5131-2009>.
- Zhang, Y., Mao, H., Ding, A., Zhou, D., Fu, C., 2013. Impact of synoptic weather patterns on spatio-temporal variation in surface O<sub>3</sub> level in Hong Kong during 1999–2011. *Atmos. Environ.* 73, 41–50. <http://dx.doi.org/10.1016/j.atmosenv.2013.02.047>.
- Zhang, Y., Wen, X.-Y., Wang, K., Vijayaraghavan, K., Jacobson, M.Z., 2009b. Probing into regional O<sub>3</sub> and particulate matter pollution in the United States: 2. An examination of formation mechanisms through a process analysis technique and sensitivity study. *J. Geophys. Res.* 114, D22305. <http://dx.doi.org/10.1029/2009JD011900>.
- Zheng, X., Wan, G., Tang, J., 2011. Source characteristics of O<sub>3</sub> and CO<sub>2</sub> at Mt. Waliguan observatory, Tibetan Plateau implied by using <sup>7</sup>Be and <sup>210</sup>Pb. *Sci. China Earth Sci.* 54 (4), 550–560.